Dynamical localization simulated on a few-qubit quantum computer

Giuliano Benenti,[1] Giulio Casati,[1,2] Simone Montangero,[1] and Dima L. Shepelyansky[3]
[1]*Center for Nonlinear and Complex Systems, Università degli Studi dell'Insubria and Istituto Nazionale per la Fisica della Materia, Unità di Como, Via Valleggio 11, 22100 Como, Italy*
[2]*Istituto Nazionale di Fisica Nucleare, Sezione di Milano, Via Celoria 16, 20133 Milano, Italy*
[3]*Laboratoire de Physique Quantique, UMR 5626 du CNRS, Université Paul Sabatier, 31062 Toulouse Cedex 4, France*
(Received 8 October 2002; published 28 May 2003)

We show that a quantum computer operating with a small number of qubits can simulate the dynamical localization of classical chaos in a system described by the quantum sawtooth map model. The dynamics of the system is computed efficiently up to a time $t \geqslant \ell$, and then the localization length ℓ can be obtained with accuracy ν by means of order $1/\nu^2$ computer runs, followed by coarse-grained projective measurements on the computational basis. We also show that in the presence of static imperfections, a reliable computation of the localization length is possible without error correction up to an imperfection threshold which drops polynomially with the number of qubits.

DOI: 10.1103/PhysRevA.67.052312 PACS number(s): 03.67.Lx, 05.45.Mt, 24.10.Cn

I. INTRODUCTION

Recent experimental progress in nuclear magnetic resonance (NMR)-based quantum processors allowed the demonstration of quantum algorithms [1], including Grover's algorithm [2] and quantum Fourier transform [3]. More recently, it has been possible to implement the simplest instance of Shor's algorithm, namely, the factorization of 15, using 7 qubits and a sequence of about 300 spin-selective radio-frequency pulses [4]. In parallel, thanks to the development of techniques for the manipulation of cold atoms in linear traps, the realization of up to 50 two-qubit controlled-NOT gates within the relevant decoherence time scale is currently becoming possible [5,6]. Solid state realizations are also under way in several experimental groups working with various solid-state devices. In particular, it has been demonstrated that a superconducting tunnel junction circuit can behave as an artificial spin-1/2 atom, whose evolution can be controlled by applying microwave pulses. The quality factor of quantum coherence is sufficiently high to envisage the realization of two-qubit gates based on capacitively coupled circuits of this type [7].

In this context, it is of primary importance to find efficient quantum algorithms, which could be usefully simulated with a small number of qubits. Such algorithms would naturally become the ideal software for demonstrative experiments in the coming generation of quantum processors. Dynamical models represent a natural testing ground for quantum information processors. The algorithm for the quantum baker's map [8] has been recently implemented on a three-qubit NMR quantum processor [9]. These experiments tested the sensitivity to perturbations, in a system that is characterized by chaotic unpredictable dynamics in the classical limit.

In this paper, we show that quantum computers can simulate efficiently the quantum localization of classical chaos. Dynamical localization is one of the most interesting phenomena that characterize the quantum behavior of classically chaotic systems: Quantum interference effects suppress chaotic diffusion in momentum, leading to exponentially localized wave functions. This phenomenon was first found and studied in the quantum kicked rotator model [10] and has profound analogies with Anderson localization of electronic transport in disordered materials [11]. Dynamical localization has been observed experimentally in the microwave ionization of the Rydberg atoms [12] and is now actively studied in experiments with cold atoms [13].

In this paper, we study dynamical localization for the quantum sawtooth map, using the algorithm developed in Ref. [14]. This algorithm has some specific advantages with respect to similar algorithms for the simulation of other dynamical systems, for instance, the kicked rotator [15]. There are no extra work space qubits, namely, all the qubits are used to simulate the dynamics of the system. This implies that less than 40 qubits would be sufficient to make simulations inaccessible to present day supercomputers. We note that this figure has to be compared with more than 1000 qubits required to Shor's algorithm to outperform classical computations. We will also show that in this model dynamical localization could be observed already with six qubits.

Finally, we will discuss the stability of quantum computing of dynamical localization in the presence of static imperfections in the quantum computer hardware. It has been pointed out in Refs. [16,17] that unwanted mutual interactions between qubits can be a source of error in quantum computation, and some characteristic features of this type of error have been studied, also in connection with error correction [18,19]. This kind of error may be relevant in practical implementations of quantum computation. For instance, in the ion-trap quantum processors [5,6], magnetic dipole-dipole interactions couple qubits. In NMR quantum computing, residual unwanted interactions survive after nonperfect spin echoes [1]. Therefore, it is important to study the stability of quantum information processing in the presence of realistic models of hardware imperfections and in concrete examples of quantum algorithm. In this paper, we determine the tolerance bounds for reliable quantum computation of the localization length. We will show that, in the presence of static imperfections, such a computation is possible without error correction up to an imperfection threshold which drops polynomially with the number of qubits.

 ©2003 The American Physical Society

The paper is organized as follows. In Sec. II, we describe the sawtooth map model, focusing on the regime of dynamical localization. In Sec. III, we show that a quantum computer operating with few qubits can indeed perform simulations of dynamical localization. In Sec. IV, we discuss how to extract information (the localization length) from the quantum computer wave function. In Sec. V, we study the stability of those computations in the presence of static imperfections in the quantum computer hardware. In Sec. VI, we discuss the transition to quantum chaos, induced by static imperfections, in the quasienergy spectral statistics. In Sec. VII, we present our conclusions.

II. THE MODEL

The quantum sawtooth map is the quantized version of the classical sawtooth map, which is given by

$$\overline{n}=n+k(\theta-\pi),\quad \overline{\theta}=\theta+T\overline{n}, \tag{1}$$

where (n,θ) are conjugated action-angle variables ($0\leqslant\theta<2\pi$), and the over bars denote the variables after one-map iteration. Introducing the rescaled momentum variable $p=Tn$, one can see that the classical dynamics depends only on the single parameter $K=kT$. The map (1) can be studied on the cylinder $[p\in(-\infty,+\infty)]$, which can also be closed to form a torus of length $2\pi L$, where L is an integer. For $K>0$, the motion is completely chaotic and exhibits normal diffusion: $\langle(\Delta p)^2\rangle\approx D(K)t$, where t is the discrete time measured in units of map iterations and the average $\langle\cdots\rangle$ is performed over an ensemble of particles with initial momentum p_0 and random phases $0\leqslant\theta<2\pi$. For $K>1$ the diffusion coefficient is well approximated by the random phase approximation, $D(K)\approx(\pi^2/3)K^2$.

The quantum evolution in one map iteration is described by a unitary operator $\hat{U}$ (called the Floquet operator) acting on the wave function ψ:

$$\overline{\psi}=\hat{U}\psi=e^{-iT\hat{n}^2/2}e^{ik(\hat{\theta}-\pi)^2/2}\psi, \tag{2}$$

where $\hat{n}=-i\partial/\partial\theta$ and $\psi(\theta+2\pi)=\psi(\theta)$ (we set $\hbar=1$). The classical limit corresponds to $k\to\infty$, $T\to0$, and $K=kT=$const. In Refs. [14,20,21], we studied map (2) in the semiclassical regime. This is possible by increasing the number of qubits $n_q=\log_2 N$ (N is the total number of levels), with $T=2\pi L/N$, $K=$const. In this way, the number of levels inside the "unit cell" $-\pi\leqslant p<\pi$ ($L=1$) grows exponentially with the number of qubits ($-N/2\leqslant n<N/2$), and the effective Planck constant $\hbar_{\rm eff}\sim\hbar/k\sim1/N\to0$ when $N\to\infty$.

Differently from previous studies, in this paper we study map (2) in the deep quantum regime of dynamical localization. For this purpose, we keep k,K constant. Thus the effective Planck constant is fixed and the number of cells L grows exponentially with the number of qubits ($L=TN/2\pi$). In this case, one studies the quantum sawtooth map on the cylinder $[n\in(-\infty,+\infty)]$, which is cut-off to a finite number of cells due to the finite quantum (or classical) computer memory. We stress again that, since in a quantum computer the memory capabilities grow exponentially with the number of qubits, already with less than 40 qubits, one could make simulations of systems inaccessible for today's supercomputers. Similar to other models of quantum chaos [10], the quantum interference in the sawtooth map leads to suppression of classical chaotic diffusion after a break time

$$t^\star\approx D_n\approx(\pi^2/3)k^2, \tag{3}$$

where D_n is the classical diffusion coefficient, measured in number of levels ($\langle(\Delta n)^2\rangle\approx D_n t$). For $t>t^\star$ only $\Delta n\sim D_n$ levels are populated and the localization length $\ell\sim\Delta n$ for the average probability distribution is approximately equal [22]:

$$\ell\approx D_n. \tag{4}$$

Thus the quantum localization can be detected if ℓ is smaller than the system size N.

In the following, we consider $K=\sqrt{2}$, two values of k, $k=\sqrt{3}$ and $k=2$, and $6\leqslant n_q\leqslant21$, so that the above analytical estimate gives $\ell(k=\sqrt{3})\approx10$ and $\ell(k=2)\approx13<N$. We assume that at $t=0$ the system is in a momentum eigenstate, $\hat{\psi}(n)=\delta_{nn_0}$. Since this is a quantum register state, it can be obtained in $O(n_q)$ one-qubit operations starting from the fiducial state ("ground state") $\overline{n}$ of the quantum computer hardware.

III. SIMULATION OF DYNAMICAL LOCALIZATION

An exponentially efficient quantum algorithm for the simulation of map (2) was developed in Ref. [14]. It is based on the forward and backward quantum Fourier transform [1] between momentum and coordinate bases. Such an approach is convenient since the Floquet operator U, introduced in Eq. (2), is the product of two operators, $\hat{U}_k=e^{ik(\hat{\theta}-\pi)^2/2}$ and $\hat{U}_T=e^{-iT\hat{n}^2/2}$, which are diagonal in the θ and n representations, respectively. Our quantum algorithm requires the following steps for one map iteration.

(i) We apply $\hat{U}_k$ to the wave function $\psi(\theta)$. In order to decompose the operator $\hat{U}_k$ in one- and two-qubit gates, we first of all write θ in binary notation:

$$\theta=2\pi\sum_{j=1}^{n_q}\alpha_j 2^{-j} \tag{5}$$

with $\alpha_i\in\{0,1\}$. From this expansion, we get

$$(\theta-\pi)^2=4\pi^2\sum_{j_1,j_2=1}^{n_q}\left(\frac{\alpha_{j_1}}{2^{j_1}}-\frac{1}{2n_q}\right)\left(\frac{\alpha_{j_2}}{2^{j_2}}-\frac{1}{2n_q}\right). \tag{6}$$

This term can be put into the unitary operator U_k, giving the decomposition

$$e^{ik(\theta-\pi)^2/2}=\prod_{j_1,j_2=1}^{n_q}e^{i2\pi^2k(\alpha_{j_1}/2^{j_1}-1/2n_q)(\alpha_{j_2}/2^{j_2}-1/2n_q)}, \tag{7}$$

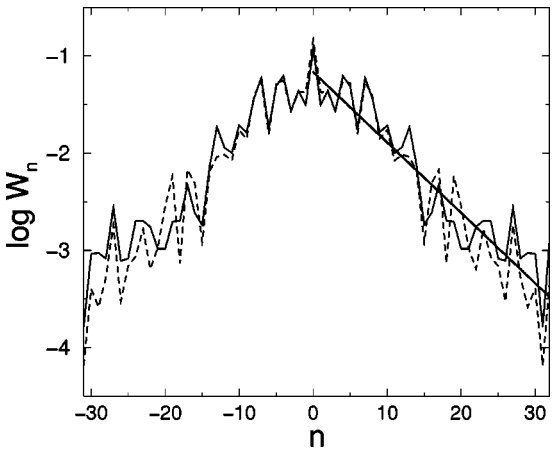

FIG. 1. Exact quantum computation of probability distribution over the momentum basis with $n_q=6$ qubits for $k=\sqrt{3}$ and initial momentum $n_0=0$; the average is taken in the intervals $10\leqslant t\leqslant 20$ (full curve) and $290\leqslant t\leqslant 300$ (dashed curve). The straight-line fit, $W_n\propto\exp(-2|n|/\ell)$, gives a localization length $\ell\approx 12$. Here and in the following figures, the logarithms are decimal.

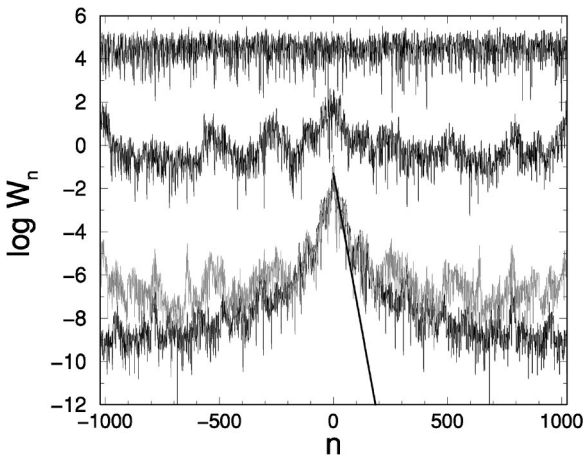

FIG. 2. Probability distributions for $k=2$, $n_q=11$, $n_0=0$, $J=0$. From bottom to top: $\epsilon=0$, 10^{-4} (gray line), 10^{-3} (shifted up by a factor of 4), and 10^{-2} (shifted up by a factor of 8). The straight line gives a localization length $\ell\approx 15$.

which is the product of n_q^2 two-qubit gates (controlled-phase shifts), each one acting nontrivially only on the qubits j_1 and j_2.

(ii) The change from the θ to the n representation is obtained by means of the quantum Fourier transform, which requires n_q Hadamard gates and $n_q(n_q-1)/2$ controlled-phase-shift gates [1].

(iii) In the n representation, the operator $\hat{U}_T$ has essentially the same form as the operator $\hat{U}_k$ in the θ representation, and therefore it can be decomposed in n_q^2 controlled-phase shift gates, similar to Eq. (7).

(iv) We go back to the initial θ representation by application of the inverse quantum Fourier transform.

Thus, on the whole the algorithm requires $n_g=3n_q^2+n_q$ gates per map iteration ($3n_q^2-n_q$ controlled-phase shifts and $2n_q$ Hadamard gates). This number has to be compared with the $O(N\ln N)$ operations required to a classical computer to simulate one map iteration by means of the fast Fourier transform.

In Fig. 1, we show that, using our quantum algorithm, exponential localization can be clearly seen already with $n_q=6$ qubits. After the break time $t^\star$, the probability distribution over the momentum eigenbasis decays exponentially,

$$W_n=|\hat{\psi}(n)|^2\approx\frac{1}{\ell}\exp\left(-\frac{2|n-n_0|}{\ell}\right), \tag{8}$$

with $n_0=0$ the initial momentum value. Here the localization length is $\ell\approx 12$, and classical diffusion is suppressed after a break time $t^\star\approx\ell$, in agreement with estimates (3)–(4). This requires a number $N_g\approx 3n_q^2\ell\sim 10^3$ of one- or two-qubit quantum gates. The full curve of Fig. 1 shows that an exponentially localized distribution indeed appears at $t\approx t^\star$. Such a distribution is frozen in time, apart from quantum fluctuations, which we partially smooth out by averaging over a few map steps. The localization can be seen by the comparison of the probability distributions taken immediately after $t^\star$ (full curve in Fig. 1) and at a much longer time $t=300\approx 25t^\star$ (dashed curve in the same figure).

We also note that the asymptotic tails of the wave-functions decay as a power law (see Fig. 2),

$$W_n\propto\frac{1}{|n-n_0|^4}. \tag{9}$$

This happens due to the discontinuity in the kicking force of Eq. (1), $f(\theta)=k(\theta-\pi)$, when the angle variable $\theta=0$. For that reason the matrix elements of the one-period evolution operator $\hat{U}$ for quantum map (2) decay as a power law in the momentum eigenbasis: $U_{nm}=\langle n|\hat{U}|m\rangle\sim 1/|n-m|^\alpha$, with $\alpha=2$. This case was investigated for random matrices, where it was shown that eigenfunctions are also algebraically localized with the same exponent α [23]. We also note that dynamical localization in discontinuous systems was studied in Ref. [24]. Since the localization picture is not very sensitive to the behavior of the tails of the wave function, a rough estimate of the crossover between the exponential decay (8) and the power-law decay (9) is given by their crossing point,

$$n_c\sim\frac{3}{2}\ell\ln\ell,\quad W_n(n_c)\sim\frac{1}{\ell^4\ln\ell}. \tag{10}$$

This implies that by increasing ℓ the exponential localization is pushed to larger momentum windows and down to smaller probabilities.

IV. MEASUREMENTS

We now discuss how it would be possible to extract information (the value of the localization length) from a quantum computer simulating the above described dynamics. The localization length can be measured by running the algorithm several times up to a time $t>t^\star$. Each run is followed by a standard projective measurement on the computational (mo-

mentum) basis. Since the wave function at time t can be written as

$$|\psi(t)\rangle = \sum_n \hat{\psi}(n,t)|n\rangle, \tag{11}$$

with $|n\rangle$ momentum eigenstates, such a measurement gives outcome $\overline{n}$ with probability

$$W_{\overline{n}} = |\langle \overline{n}|\psi(t)\rangle|^2 = |\hat{\psi}(\overline{n},t)|^2. \tag{12}$$

A first series of measurements would allow us to give a rough estimate of the variance $\langle(\Delta n)^2\rangle$ of the distribution W_n. In turn, $\sqrt{\langle(\Delta n)^2\rangle}$ gives a first estimate of the localization length ℓ. After that, we can store the outcomes of the measurements in histogram bins of width $\delta n \propto \ell \approx \sqrt{\langle(\Delta n)^2\rangle}$. Finally, the localization length is extracted from a fit of the exponential decay of this coarse-grained distribution over the momentum basis. Elementary statistical theory tells us that, in this way, the localization length can be obtained with accuracy ν after the order of $1/\nu^2$ computer runs. It is important to note that it is sufficient to perform a coarse grained measurement to generate a coarse-grained distribution. This means that it will be sufficient to measure the most significant qubits, and ignore those that would give a measurement accuracy below the coarse-graining δn. Thus, the number of runs and measurements is independent of ℓ.

We now come to the crucial point, of estimating the gain of quantum computation of the localization length with respect to classical computation. First of all, we recall that it is necessary to make about $t^\star \sim \ell$ map iterations to obtain the localized distribution [see Eqs. (3) and (4)]. This is true, both for the present quantum algorithm and for classical computation. It is reasonable to use a basis size $N \propto \ell$ to detect localization (let us say N equal to a few times the localization length). In such a situation ($N \sim \ell$), a classical computer needs $O(\ell^2 \ln \ell)$ operations to extract the localization length, while a quantum computer would require $O(\ell(\ln \ell)^2)$ elementary gates. In this sense, for $\ell \sim N = 2^{n_q}$ the quantum computer gives a *quadratic speed up*, since both classical and quantum computers perform $O(N)$ map iterations. However, for a fixed number of iterations t the quantum computation gives an *exponential gain*, since, in this case, one should compare $O(t(\ln N)^2)$ gates (quantum computation) with $O(tN \ln N)$ gates (classical computation). We note that, as explained above, these quantum simulations up to time t can also be used to estimate the variance $\langle(\Delta n(t))^2\rangle$. From this quantity, it is possible to get an important characteristic related to the transport properties of the system, namely, the diffusion coefficient $D_n \approx \langle(\Delta n(t))^2\rangle/t$.

Finally, we note that in more complex transport problems, quantum computation of the localization length could provide new important physical insights. Indeed, the quantum computer has enormous memory capabilities, since the size of the Hilbert space grows exponentially with the number of qubits. This would be very useful in the study of complex many-body systems. In these problems, it would be highly desirable to access huge Hilbert-space dimensions, in order to check if a system is truly localized. We also note that this is a difficult task not only in many-body quantum systems, but also in single-particle models such as the Harper model [25].

V. EFFECTS OF STATIC IMPERFECTIONS

In order to study the effects of static imperfections on the stability of the above described algorithm, we model the quantum computer hardware as a linear array of qubits with static imperfections, represented by fluctuations in the individual qubit energies and residual short-range interqubit couplings [17]. The model is described by the following many-body Hamiltonian:

$$\hat{H}_s = \sum_i (\Delta_0 + \delta_i)\hat{\sigma}_i^z + \sum_{i<j} J_{ij}\hat{\sigma}_i^x\hat{\sigma}_j^x, \tag{13}$$

where the $\hat{\sigma}_i i$'s are the Pauli matrices for the qubit i, and Δ_0 is the average level spacing for one qubit. The second sum in Eq. (13) runs over nearest-neighbor qubit pairs, zero boundary conditions are applied, and δ_i, J_{ij} are randomly and uniformly distributed in the intervals $[-\delta/2, \delta/2]$ and $[-J, J]$, respectively. We model the implementation of the above algorithm on this hardware architecture as a sequence of instantaneous and perfect one- and two-qubit gates, separated by a time interval τ_g. Therefore, we study numerically the evolution in the time of the quantum computer wave function in the presence of the following many-body Hamiltonian:

$$\hat{H}(\tau) = \hat{H}_s + \hat{H}_g(\tau), \tag{14}$$

where

$$\hat{H}_g(\tau) = \sum_k \delta(\tau - k\tau_g)\hat{h}_k. \tag{15}$$

Here $\hat{h}_k$ realizes the kth elementary gate according to the sequence prescribed by the algorithm. We assume that the phase accumulation given by Δ_0 is eliminated by standard spin echo techniques [1]. In this case, the remaining terms in the static Hamiltonian (13) can be seen as residual terms after imperfect spin echoes [1] and give unwanted phase rotations and qubit couplings.

The effect of static imperfections on the probability distribution over the momentum basis is shown in Fig. 2, for $k = 2$, $n_q = 11$, $t = 100$, $J = 0$, and different rescaled imperfection strengths $\epsilon = \delta\tau_g$. For $\epsilon = 10^{-4}$, the localization peak is reproduced with high fidelity, while the tails of the wave function are strongly enhanced. This is due to the fact that errors affecting the most significant qubits can induce a direct transfer of probability very far in the momentum basis [26,14]. For $\epsilon = 10^{-3}$, a measurement of the decay of the localization peak would overestimate the localization length by a factor of 2, while for $\epsilon = 10^{-2}$, any trace of dynamical localization has been destroyed.

In order to study in a more quantitative way the stability of quantum computation in the presence of static imperfections, we consider the following two quantities.

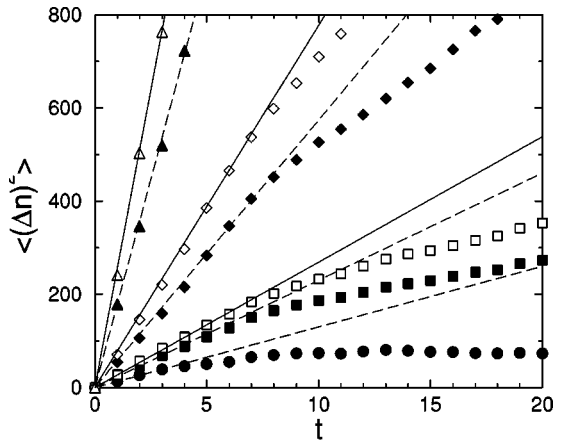

FIG. 3. Dependence of the wave-function second moment on time, for $k=2$, $n_q=11$, $J=0$ (full symbols), and $J=\delta$ (empty symbols) at $\epsilon=0$ (circles), 5×10^{-5} (squares), 10^{-4} (diamonds), and 2×10^{-4} (triangles). The straight line fits give the diffusion coefficient $D_n(\epsilon)$. The curves are averaged over 10 disorder realizations and 10 initial conditions $n_0\in[-5,5[$.

(i) The diffusion coefficient $D_n(\epsilon)$, obtained from the relation

$$\langle(\Delta n)^2\rangle\approx D_n(\epsilon)t. \tag{16}$$

This is an important characteristic related to transport properties of the system;

(ii) The inverse participation ratio

$$\xi=\frac{1}{\Sigma_n W_n^2}; \tag{17}$$

this quantity determines the number of basis states significantly populated by the wave function and gives an estimate of the localization length of the system. We stress that, differently from the previous quantity, ξ is local in the localized regime, i.e., it is insensitive to the behavior of exponentially small tails.

In Fig. 3 we show $\langle(\Delta n)^2\rangle$ as a function of time, for $n_q=11$ qubits, $J=0$, and different imperfection strengths ϵ. By means of these curves we extract the diffusion coefficients $D_n(\epsilon)$ from linear fits extended to the first few map steps. In the same figure, we show that similar curves are obtained for $J=\delta$. The dependence of the inverse participation ratio on t is shown in Fig. 4, again for $k=2$, $n_q=11$. We note that, for imperfection strengths strong enough to induce huge variations in the diffusion coefficient ($D_n(\epsilon)\gg D_n(0)$), ξ is only slightly modified [$\xi(\epsilon)\approx\xi(0)$]. Iterating map (2) long enough [$t>\xi(\epsilon)$], we get the saturation value $\xi_\infty(\epsilon)$. This quantity increases with ϵ and one has complete delocalization when $\xi_\infty(\epsilon)\sim N$ (this is evident for $\epsilon=5\times10^{-3}$ in Fig. 4; in this case ξ saturates after $t<100$ map iterations). Again, we note that similar curves are obtained for $J=\delta$ (see Fig. 4).

In Fig. 5, we plot the dependence of diffusion coefficient D_n on ϵ for different n_q values. From each curve we extract the critical imperfection strength $\epsilon_D(n_q)$ corresponding to

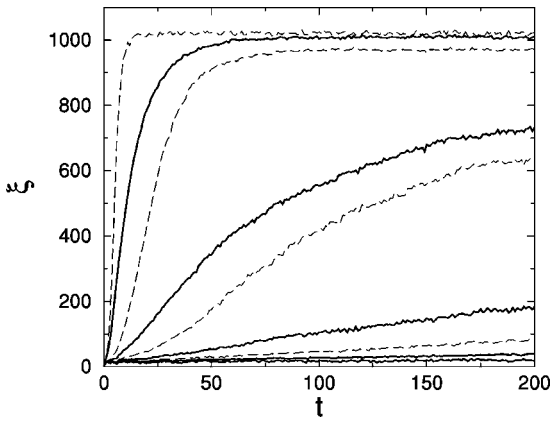

FIG. 4. Time dependence of the inverse participation ratio ξ for $k=2$, $n_q=11$ qubits, $J=0$ (solid lines), and $J=\delta$ (dashed lines). From bottom to top: $\epsilon=0$, 5×10^{-4}, 10^{-3}, 2×10^{-3}, 5×10^{-3}. The curves are averaged as in Fig. 3.

doubling of the diffusion coefficient $D_n(\epsilon_D)=2D_n(0)$. The data of Fig. 7 show that ϵ_D drops exponentially with n_q. This result is similar to that found in Ref. [26] for noisy gate errors and can be explained by means of the following argument. Static imperfections can couple states very far in momentum space via a single spin flip. As a consequence, they create n_q peaks [26] with probability $W_p\sim\epsilon_{\rm eff}^2 t$ in each peak. Here $\epsilon_{\rm eff}\sim\delta n_q^2\tau_g=\epsilon n_q^2$ is the effective perturbation strength, with $n_q^2\tau_g$ time between the Hadamard gates acting on a given qubit. These gates transfer the accumulated phase error $\epsilon_{\rm eff}$ into amplitude errors. Integrating the contribution of each peak, one gets

$$\langle(\Delta n)^2\rangle\sim W_p N^2\sim\overline{D}_\epsilon t \tag{18}$$

with

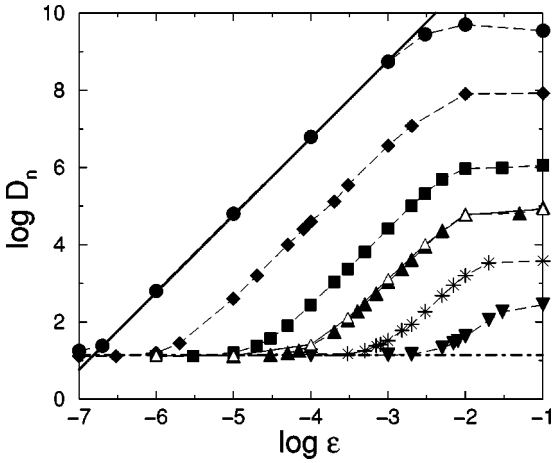

FIG. 5. Dependence of the diffusion coefficient D_n on the imperfection strength ϵ for $k=2$, $J=0$ (full symbols), $n_q=6$ (triangles down), 8 (stars), 10 (triangles up), 12 (squares), 15 (diamonds), 18 (circles), and for $J=\delta$, $n_q=10$ (empty triangles). The straight lines show the theoretical dependence $D\propto\epsilon^2$ [full line, see Eq. (19)] and the result without imperfections, $D(\epsilon=0)\approx16$ (chain line).

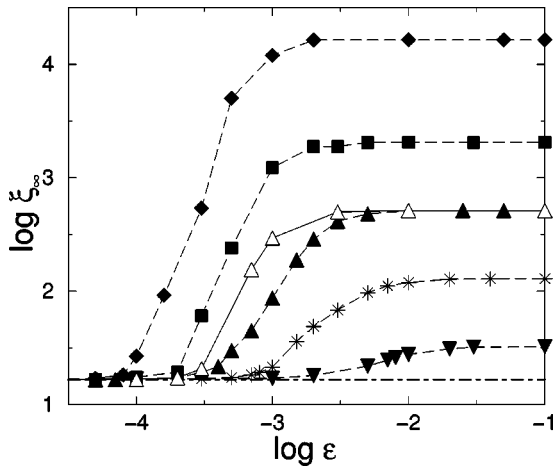

FIG. 6. Dependence of the saturation value ξ_∞ of the inverse participation ratio on the imperfection strength ϵ, with same parameter values and same meaning of symbols as in the previous figure. The straight line shows the result without imperfections, $\xi_\infty(\epsilon=0)\approx 14$.

$$\overline{D}_\epsilon \sim \epsilon^2 n_q^4 N^2. \tag{19}$$

One can estimate the critical value ϵ_D to double the exact $(\epsilon=0)$ diffusion coefficient from $\overline{D}_\epsilon = D_n(\epsilon=0)$, giving

$$\epsilon_D \sim \frac{\sqrt{D_n(0)}}{n_q^2 N}, \tag{20}$$

in good agreement with the data of Fig. 7.

In Fig. 6 we show the dependence of the inverse participation ratio $\xi(\epsilon)$ on ϵ for different number of qubits n_q. From each curve, we extract two critical imperfection strengths.

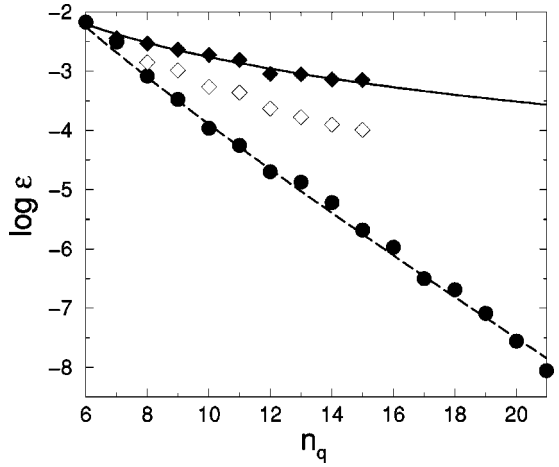

FIG. 7. Dependence of the critical imperfection strengths on the number of qubits for $k=2$, $J=0$: thresholds ϵ_D (circles), $\epsilon_{\xi E}$ (full diamonds), and ϵ_ξ (empty diamonds). The full line gives the theoretical dependence $\epsilon_{\xi E} = A n_q^{-5/2}$, with the fitting constant $A\approx 0.5$. The dashed lines give $\epsilon_D = B\sqrt{D(\epsilon=0)}\,2^{-n_q} n_q^{-2}$, with the fitting constant $B\approx 3.6$.

(i) $\epsilon_{\xi E}$, to get an inverse participation ratio equal to a given fraction of the full Hilbert space, for example, $\xi = N/4$. This threshold characterizes the transition to ergodic completely delocalized wave functions.

(ii) ϵ_ξ, to double the exact inverse participation ratio. We stress that this quantity gives a rough estimate of the imperfection threshold for reliable quantum computation of localization in the absence of error correction.

The dependence of $\epsilon_{\xi E}$ and ϵ_ξ on n_q is shown in Fig. 7. These quantities drop polynomially with n_q, in sharp contrast with the exponential drop of ϵ_D. This algebraic threshold can be understood as follows. The eigenstates of the unperturbed $(\epsilon=0, J=0)$ Floquet operator $\hat{U}$ in Eq. (2) can be written as

$$\phi_\alpha^{(0)} = \sum_{m=1}^{N} c_\alpha^{(m)} u_m, \tag{21}$$

where u_m are the quantum register (momentum) states. In the localized regime, $c_\alpha^{(m)}$'s are randomly fluctuating inside the localization domain of size ℓ, and exponentially small outside it. Wave-function normalization imposes $|c_\alpha^{(m)}| \sim 1/\sqrt{\ell}$. Due to exponential localization, static imperfections couple significantly the unperturbed eigenfunctions only when their localization domains overlap. We estimate in this case the transition matrix elements according to perturbation theory. For $J=0$, they have a typical value

$$\begin{aligned} V_{\rm typ} &\sim |\langle \phi_\beta^{(0)}| \sum_{i=1}^{n_q} \delta_i \hat{\sigma}_i^z \tau_g n_g |\phi_\alpha^{(0)}\rangle| \\ &\sim \tau_g n_q^2 \Big| \sum_{m,n=1} \ell\, c_\alpha^{(m)} c_\beta^{(n)\star} \sum_{i=1}^{n_q} \delta_i \langle u_n|\hat{\sigma}_i^z|u_m\rangle \Big| \\ &\sim \epsilon n_q^{5/2} \Big| \sum_{m=1} \ell\, c_\alpha^{(m)} c_\beta^{(m)\star} \eta^{(m)} \Big| \sim \epsilon n_q^{5/2} \ell^{-1/2}. \end{aligned} \tag{22}$$

In this expression, the typical phase error is $\delta\sqrt{n_q}\eta^{(m)}$ (sum of n_q random detunings δ_i's), with $\eta^{(m)}$ random sign, and $\tau_g n_g \sim \tau_g n_q^2$ is the time taken by the quantum computer to simulate one map step. The last estimate in Eq. (22) results from the sum of order ℓ terms of amplitude $|c_\alpha^{(m)} c_\beta^{(m)\star}| \sim 1/\ell$ and random phases. Since the spacing between significantly coupled quasienergy eigenstates is $\Delta E \sim 1/\ell$, the threshold for the breaking of perturbation theory can be estimated as

$$V_{\rm typ}/\Delta E \sim \epsilon_{\xi E} n_q^{5/2} \sqrt{\ell} \sim 1. \tag{23}$$

The analytical result

$$\epsilon_{\xi E} \sim \frac{1}{n_q^{5/2}\sqrt{\ell}} \tag{24}$$

is confirmed by the numerical data of Fig. 7. For the case $J=\delta$, the threshold $\epsilon_{\xi E}$ is reduced (see Fig. 4) since residual interqubit interactions introduce further couplings between the Floquet eigenstates. However, an estimate similar to Eq.

(22), which does not modify the functional dependence (23), can be derived. We stress the striking difference between this polynomial scaling and the exponential scaling for the mixing of unperturbed eigenstates obtained in the ergodic regime (in which $\ell \sim N$) and in the more general quasi-integrable regime [20,21]. We also note that the different sensitivity of local and nonlocal quantities was pointed out in Ref. [26]. However, the authors of Ref. [26] considered the effect of noisy gates, while we consider internal static imperfections.

VI. SPECTRAL STATISTICS

In this section, we show that spectral statistics is an ideally suited tool to detect the destruction of localization by static imperfections. We study the spectral statistics of the Floquet operator for a quantum computer running the quantum sawtooth map algorithm in the presence of static imperfections,

$$\hat{U}_\epsilon = \exp\left(-i \int_0^{\tau_g n_g} d\tau \hat{H}(\tau) \right), \tag{25}$$

where $H(\tau)$ is the Hamiltonian (14) and n_g is the number of gates per map iteration. We construct numerically the Floquet operator in the computational (momentum) basis, using the fact that a single-map iteration of each quantum register state gives a column in the matrix representation of this operator. Then we diagonalize the Floquet matrix and get the so-called quasienergy eigenvalues $\lambda_\alpha^{(\epsilon)}$ and eigenvectors $\phi_\alpha^{(\epsilon)}$,

$$\hat{U}_\epsilon \phi_\alpha^{(\epsilon)} = \exp(i\lambda_\alpha^{(\epsilon)}) \phi_\alpha^{(\epsilon)}. \tag{26}$$

A convenient way to characterize the spectral properties of the system is to study the level spacing statistics $P(s)$, where $P(s)ds$ gives the probability to find two adjacent levels (quasienergies) whose energy difference, normalized to the average level spacing, belongs to the interval $[s, s+ds]$ (see, e.g., Refs. [27,28]). In the localized regime, the Floquet eigenvectors with very close eigenvalues may lay so far apart that their overlap is negligible. As a consequence, eigenvalues are uncorrelated, that is, their spectral statistic is given by the Poisson distribution,

$$P_P(s) = \exp(-s). \tag{27}$$

On the contrary, in the delocalized regime wave functions are ergodic, and their overlap gives a significant coupling matrix element between states nearby in energy. In this case, the spectral statistics $P(s)$ follows the Wigner-Dyson distribution

$$P_{WD}(s) = \frac{32s^2}{\pi^2} \exp\left(-\frac{4s^2}{\pi} \right), \tag{28}$$

typical of random matrices in the absence of time-reversal symmetry [27,28] (static imperfections break this symmetry). In Fig. 8, we show that static imperfections indeed induce a crossover from the localized regime with the Poisson statistics to quantum chaos characterized by the Wigner-Dyson statistics. We have also studied this crossover as a function of the number of qubits (data not shown): the threshold $\epsilon_c(n_q)$ for the emergence of quantum chaos is consistent with the scaling $\epsilon_c(n_q) \propto n_q^{-5/2}$, in agreement with the threshold (24) obtained for the mixing of unperturbed eigenfunctions.

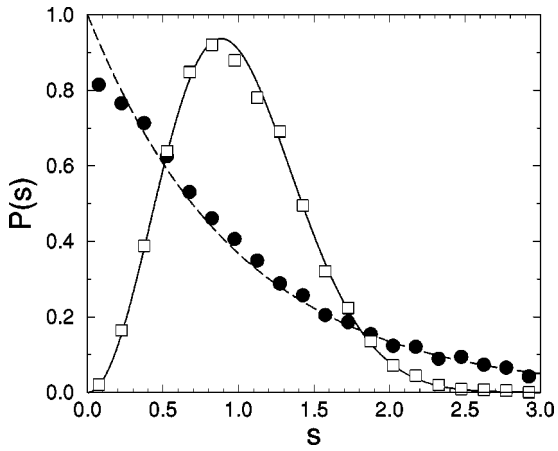

FIG. 8. Level spacing statistics for $k=2$, $n_q=11$, $J=0$, $\epsilon = 10^{-5}$ (circles), and $\epsilon = 2.6\times 10^{-3}$ (squares). The dashed and full curves give the Poisson (27) and the Wigner-Dyson distributions (28), respectively. In order to reduce statistical fluctuations, data are averaged over $N_D=5$ random realizations of δ_i's, so that the total number of spacings is $N_D N \approx 10^4$.

VII. CONCLUSIONS

In summary, we have shown that a quantum computer operating with a small number of qubits can simulate efficiently the quantum localization effects. The evaluation of the localization length ℓ with accuracy ν requires a number of computer runs of order $1/\nu^2$, followed by a projective measurement in the computational (momentum) basis. We stress that, in the presence of static imperfections, a reliable computation of the localization length is possible even without quantum error correction, up to an imperfection strength threshold that drops only algebraically with the number of qubits. We also stress that localization is a purely quantum phenomenon, which is quite fragile in the presence of noise [29,26]. Therefore, we believe that the simulation of the physics of localization can be an interesting testing ground for the coming generation of quantum processors operating in the presence of decoherence and static imperfections.

This research was supported in part by the EC RTN Contract No. HPRN-CT-2000-0156, the NSA and ARDA under ARO Contracts No. DAAD19-01-1-0553 and No. DAAD19-02-1-0086, the project EDIQIP of the IST-FET program of the EC, and the PRIN-2000 ''Chaos and localization in classical and quantum mechanics.''

[1] See, e.g., M.A. Nielsen and I.L. Chuang, *Quantum Computation and Quantum Information* (Cambridge University Press, Cambridge, 2000).
[2] L.M.K. Vandersypen, M. Steffen, M.H. Sherwood, C.S. Yannoni, G. Breyta, and I.L. Chuang, Appl. Phys. Lett. **76**, 646 (2000).
[3] Y.S. Weinstein, M.A. Pravia, E.M. Fortunato, S. Lloyd, and D.G. Cory, Phys. Rev. Lett. **86**, 1889 (2001).
[4] L.M.K. Vandersypen, M. Steffen, G. Breyta, C.S. Yannoni, M.H. Sherwood, and I.L. Chuang, Nature (London) **414**, 883 (2001).
[5] D. Leibfried, C. Roos, P. Barton, H. Rohde, S. Gulde, A.B. Muindt, G. Reymond, M. Lederbauer, F. Schmidt-Kaler, J. Eschner, and R. Blatt, in *Atomic Physics XVII*, edited by E. Arimondo, P. De Natale, and M. Inguscio AIP Conf. No. 551 (AIP, Melville, NY, 2001).
[6] S. Gulde, M. Riebe, G.P.T. Lancaster, C. Becher, J. Eschner, H. Häffner, F. Schmidt-Kaler, I.L. Chuang, and R. Blatt, Nature (London) **421**, 48 (2003).
[7] D. Vion, A. Aassime, A. Cottet, P. Joyez, H. Pothier, C. Urbina, D. Esteve, and M.H. Devoret, Science (Washington, DC, U.S.) **296**, 886 (2002).
[8] R. Schack, Phys. Rev. A **57**, 1634 (1998).
[9] Y.S. Weinstein, S. Lloyd, J.V. Emerson, and D.G. Cory, Phys. Rev. Lett. **89**, 157902 (2002).
[10] G. Casati, B.V. Chirikov, J. Ford, and F.M. Izrailev, Lect. Notes Phys. **93**, 334 (1979); for a review see, e.g., F.M. Izrailev, Phys. Rep. **129**, 299 (1990).
[11] S. Fishman, D.R. Grempel, and R.E. Prange, Phys. Rev. Lett. **49**, 509 (1982).
[12] P.M. Koch and K.A.H. van Leeuwen, Phys. Rep. **255**, 289 (1995), and references therein.
[13] F.L. Moore, J.C. Robinson, C.F. Barucha, B. Sundaram, and M.G. Raizen, Phys. Rev. Lett. **75**, 4598 (1995); H. Ammann, R. Gray, I. Shvarchuck, and N. Christensen, *ibid.* **80**, 4111 (1998); D.A. Steck, W.H. Oskay, and M.G. Raizen, *ibid.* **88**, 120406 (2002); M.E.K. Williams, M.P. Sadgrove, A.J. Daley, R.N.C. Gray, S.M. Tan, A.S. Parkins, R. Leonhardt, and N. Christensen, e-print quant-ph/0208090.
[14] G. Benenti, G. Casati, S. Montangero, and D.L. Shepelyansky, Phys. Rev. Lett. **87**, 227901 (2001).
[15] B. Georgeot and D.L. Shepelyansky, Phys. Rev. Lett. **86**, 2890 (2001).
[16] J. Gea-Banacloche, Phys. Rev. A **57**, R1 (1998); **60**, 185 (1999).
[17] B. Georgeot and D.L. Shepelyansky, Phys. Rev. E **62**, 3504 (2000); **62**, 6366 (2000); G. Benenti, G. Casati, and D.L. Shepelyansky, Eur. Phys. J. D **17**, 265 (2001).
[18] J. Gea-Banacloche, Phys. Rev. A **62**, 062313 (2000).
[19] P.G. Silvestrov, H. Schomerus, and C.W.J. Beenakker, Phys. Rev. Lett. **86**, 5192 (2001).
[20] G. Benenti, G. Casati, S. Montangero, and D.L. Shepelyansky, Eur. Phys. J. D **20**, 293 (2002).
[21] G. Benenti, G. Casati, S. Montangero, and D.L. Shepelyansky, Eur. Phys. J. D **22**, 285 (2003).
[22] D.L. Shepelyansky, Physica D **28**, 103 (1987).
[23] A.D. Mirlin, Y.V. Fyodorov, F.-M. Dittes, J. Quezada, and T.H. Seligman, Phys. Rev. E **54**, 3221 (1996).
[24] F. Borgonovi, G. Casati, and B. Li, Phys. Rev. Lett. **77**, 4744 (1996); F. Borgonovi, *ibid.* **80**, 4653 (1998); G. Casati and T. Prosen, Phys. Rev. E **59**, R2516 (1999).
[25] T. Prosen, I.I. Satija, and N. Shah, Phys. Rev. Lett. **87**, 066601 (2001), and references therein.
[26] P.H. Song and D.L. Shepelyansky, Phys. Rev. Lett. **86**, 2162 (2001).
[27] O. Bohigas, in *Les Houches Lecture Series*, edited by M.J. Giannoni, A. Voros, and J. Zinn-Justin (North-Holland, Amsterdam, 1991), Vol. 52.
[28] T. Guhr, A. Müller-Groeling, and H.A. Weidenmüller, Phys. Rep. **299**, 189 (1998).
[29] E. Ott, T.M. Antonsen, Jr., and J.D. Hanson, Phys. Rev. Lett. **53**, 2187 (1984).